

Comparison of fire spalling damage between a prestressed concrete beam and a ring restraint specimen at long curing ages

**Hiroyuki Ikeya¹⁾, Mitsuo Ozawa²⁾, Kentaro Fujimoto³⁾, Michika Hashida⁴⁾*

*1)2)4) Department of Environmental Engineering Science, Gunma University, 1-5-1,
Tenji-cho, Kiryu, Gunma, 376-8515, Japan*

3)P.S. Mitsubishi Construction Co., Ltd., 2-5-24, Harumi, Chiyoda-ku, Tokyo, 104-8572, Japan

2) ozawa@gunma-u.ac.jp

ABSTRACT

Compared to reinforced concrete structures, prestressed concrete (PC) structures have a higher risk of fire spalling because of the initial compressive stress effect due to the prestressing force. The concrete fire spalling mechanism has been discussed previously in the research literature. However, it is also necessary to consider the effects of curing age on the concrete's fire spalling behavior. Although our group reported fire spalling damage on a PC beam at 3 months there are few reports on the fire spalling of PC beams at longer curing ages. A concrete fire spalling evaluation method has been standardized by the Japan Concrete Institute. In this research, the PC beam and ring restraint specimen were both made with the same concrete mixture. A heating test was carried out on each specimen at a curing age of 24 months. We compared the fire spalling behavior between the PC beam and ring-restraint specimens. The results of the experiment showed that the maximum fire spalling depths of the ring restraint specimen were greater than those of the PC beam.

1. INTRODUCTION

Prestressed concrete (PC) can control the tensile stress and crack width that occur in concrete by introducing an initial compressive force. As a result, the PC structure has a higher mechanical performance than the reinforced concrete (RC) structures. It contributes to the large-scale and lightweight concrete structures. Therefore, PC structures are widely used not only in civil engineering structures, such as bridges and tunnels, but also in architecture building structures. Various previous studies have shown that fire spalling can occur when PC structures are exposed to high temperatures due to fire. Previous reports (Colin et al., 2009, Gales et al., 2011, Na-Hyun et al., 2015, Fujimoto et al., 2018) have shown that PC has a higher risk of fire spalling during fires compared to RC, and the risk increases with the increase in the amount of prestress

¹⁾ Graduate student

²⁾ Associate Professor, Dr.Eng.

³⁾ Company employee Ph.D.

⁴⁾ Undergraduate student

introduced. The Japan Concrete Institute Technical Committee (JCI) previously examined the fire spalling of concrete under high-temperature conditions (ref. JCI-TC154A) (Ozawa et al 2017a) and standardized the ring restraint heating test (Japan Concrete Institute, 2018). The ring restraint specimen heating test has been developed (Ozawa et al 2017b, Akasaka et al 2018).

However, there are few reports comparing the fire spalling behavior between PC beams and ring restraint specimens. Our group has reported on the examination of fire spalling of PC beams and ring restraint specimens (Ikeya et al., 2019). Although recent papers had only considered cases where the specimens were cured for 3 months, it is necessary to examine the fire spalling behavior to consider effect of the concrete curing age. In this study, we conducted a heating test to compare the fire spalling behavior of the PC beam and ring restraint specimens at 24 months. We also tried to consider the fire spalling mechanism using the relationship between restraint stress, vapor pressure, and temperature in the ring restraint specimen.

2. OVERVIEW OF EXPERIMENT

2.1 Properties of concrete

Table 1 shows the mix proportion of the concrete. The water-to-cement ratio was 0.335. One of the fine aggregates (S1) was river sand and the other (S2) was crash stone sand. The coarse aggregate (G) was granite stone. Table 2 shows the compressive strength, water content, and fresh properties of the concrete used for both specimens.

Table 1 Mix proportion

Water cement ratio	Fine aggregate ratio (%)	Unit weight (kg/m ³)					
		Water	Cement	S1	S2	G	Admixture
0.335	38.9	165	493	454	192	1045	394

Table 2 Compressive strength, water content and fresh properties of concrete

Compressive strength (N/mm ²)	Water content ratio (%)	Fresh property		
		Air content ratio (%)	Slump (cm)	Temperature (°C)
85.5	3.3	4.5	12	23.7

2.2 PC beam

Fig. 1 shows the shape and dimensions of the PC beam specimen. The PC beams were 200 mm wide, 200 mm high, and 1500 mm long. The cross section of the heating area is 200 mm wide and 160 mm high. The prestressing steel used was 17 mm in diameter (SBPR930/1080). The longitudinal reinforcement was D10 (nominal diameter: 10 mm, steel deformed bar, yield point 345 MPa), and stirrups were D6 (nominal diameter: 6 mm, steel deformed bar, yield point 295 MPa). At the outer surface of the PC beam, six thermocouples were attached 5, 10, 20, 40, 60 and 125 mm from the heated surface.

The specimen was wet-cured for the first three days. On the second day after casting, the specimen was introduced to prestressed force. The tension of the PC steel bar was a post-tension system with a hydraulic jack. The initial prestressing force was 113.5 kN, such that 5 N/mm² compressive stress is generated at the center of the bottom surface of the specimen. After that, the specimen was air-cured for approximately 24 months in the laboratory.

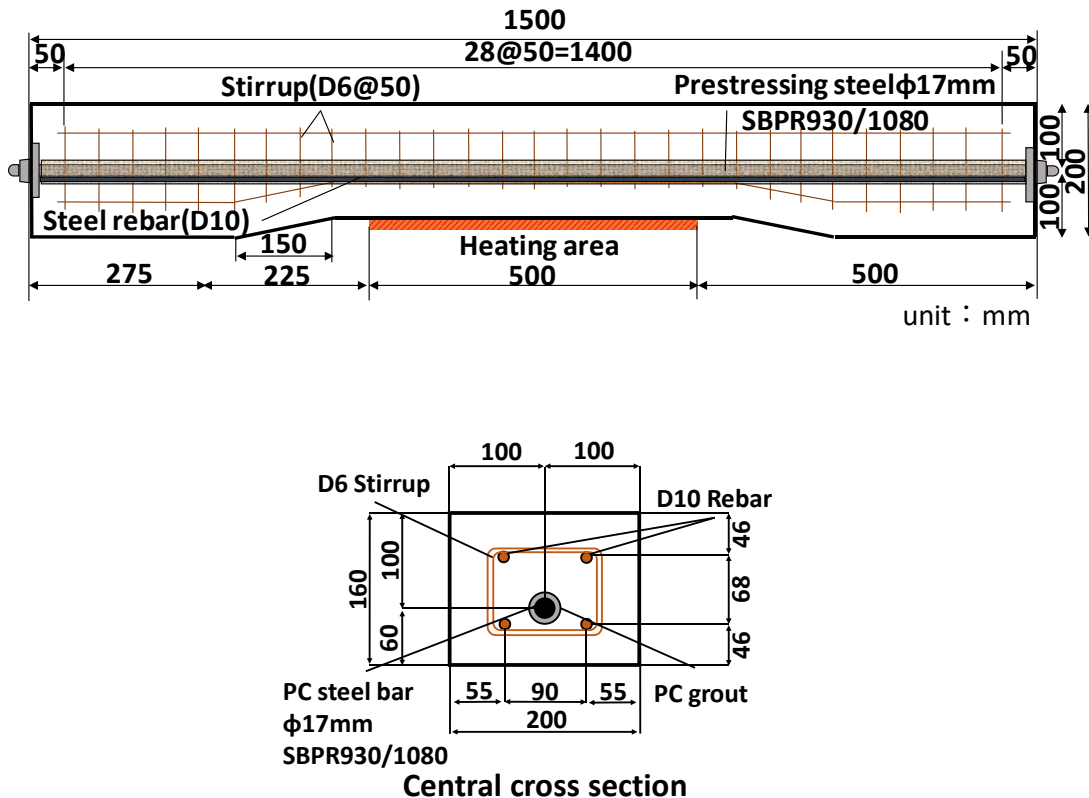


Fig. 1 The shape and dimensions of the PC beam specimen.

2.3 Ring restraint specimen

Fig. 2 shows an outline of the ring restraint specimen, fabricated with two pairs of steel rings (outer diameter: 300 mm; height: 50 mm; thickness: 8 mm). At the outer surface of the rings, four strain gauges and four thermocouples were attached 5, 10, 25, and 40 mm from the heated surface, and stainless steel pipes (outer diameter: 5 mm; inner diameter: 2 mm; length: 170 mm) were placed in the concrete parallel to the heated surface at 5, 10, 25, and 40 mm. Four thermocouples were placed in the central zone of specimens 5, 10, 25, and 40 mm from the heated surface. Similar to the PC beam, the ring restraint specimen was wet-cured for the first three days and air-cured for approximately 24 months in the laboratory.

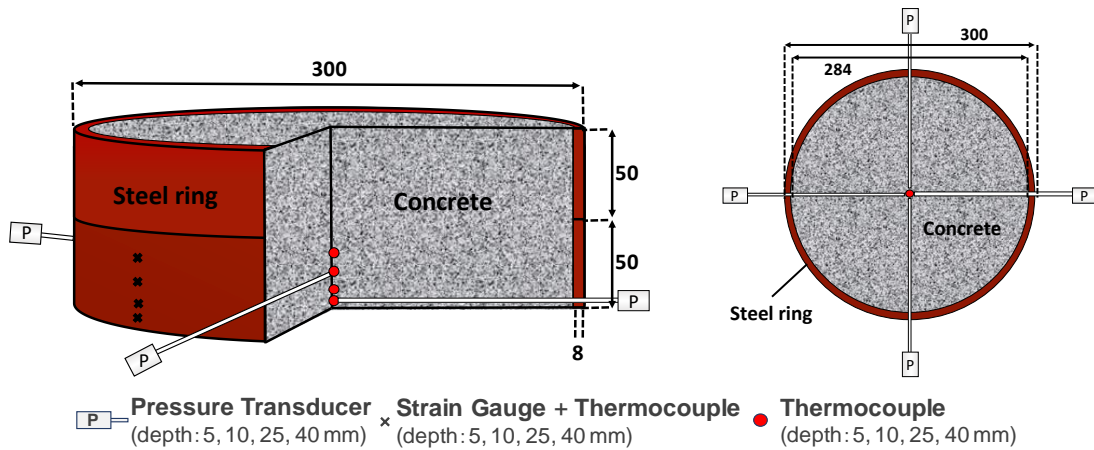


Fig. 2 Outline of ring restraint specimen

2.4 Heating test

Fig. 3 shows a high-performance horizontal gas furnace. The heating area was 900 mm square. Fig. 4 shows the RABT 30 rapid heating curve. The bottom of the specimen was heated. The specimens were covered with insulation blankets to control the temperature rise in the non-heating area. Fire spalling was observed based on sounds of spalling and peeling off the concrete pieces from the scuttle of the gas furnace. After the fire test, the extent and depth of the spalling were measured using thickness meters.

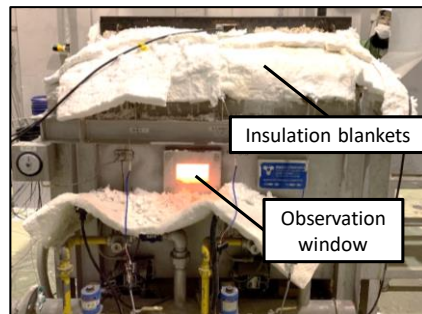


Fig. 3 The high-performance horizontal gas furnace

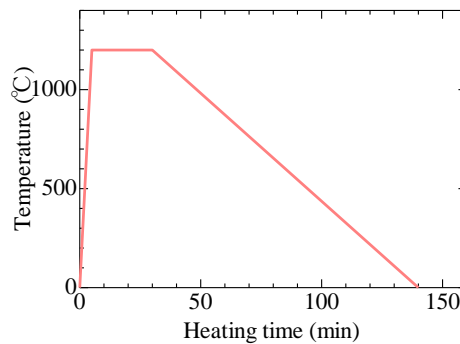


Fig. 4 RABT30 rapid heating curve

2.5 Restraint stress calculation

Restraint stress was calculated using the strain measured from the steel ring in the circumferential direction, as detailed in Eq. (1).

$$\sigma_{re} = \varepsilon_{\theta} \cdot E_s \cdot t/R \quad (1)$$

σ_{re} : Restraint stress (N/mm²)

ε_{θ} : Strain on steel ring in the circumferential direction

E_s : Elastic modulus of steel ring (N/mm²)

t : Thickness steel ring (mm)

R : Radius steel ring (mm)

2.6 Spalling evaluation from JCI standard [JCI2018]

Table. 3 shows the grading index of fire spalling. JCI has proposed the grading index to evaluate fire spalling. Index 1 is “Maximum spalling depth”, Index 2 is “Spalling area ratio” and Index 3 is “Spalling volume ratio”. This study followed this grading index.

Table. 3 the grading index of fire spalling

	Index 1 <i>Maximum spalling depth</i>	Index 2 <i>Spalling area ratio</i>	Index 3 <i>Spalling volume ratio</i>
A	No spalling, No cracks	No spalling, No cracks	No spalling, No cracks
B	Occurring only cracks	Occurring only cracks	Occurring only cracks
C	<10 mm	<10%	<10%
D	<30 mm	<50%	<20%
E	≥30 mm	≥50%	≥20%

Spalling area ratio :(area of fire spalling occurrence / heating area)

Spalling volume ratio: (Spalling volume / Specimen volume)

3. RESULT AND DISCUSSION

3.1 Fire spalling condition

Fig. 5 shows the condition of the heating surface after heating and the spalling depth contours. On the PC beam, fire spalling occurred during the fire test. It started at about 4.5 min. The maximum spalling depth was 19.9 mm, and cracks occurred up to about half the height of the PC beam’s cross section. On the other hand, on the ring restraint specimen, the spalling starting time was 4.5 min, and the maximum spalling depth was 26.0 mm. Based on these results, the fire spalling damage of the ring restraint specimen is greater than that of the PC beam. This is considered to be caused by differences in the restraint type. The PC beam is restricted in the uni-axial direction by prestress, whereas the ring restraint specimen is restricted in multi-axial directions by a steel ring.

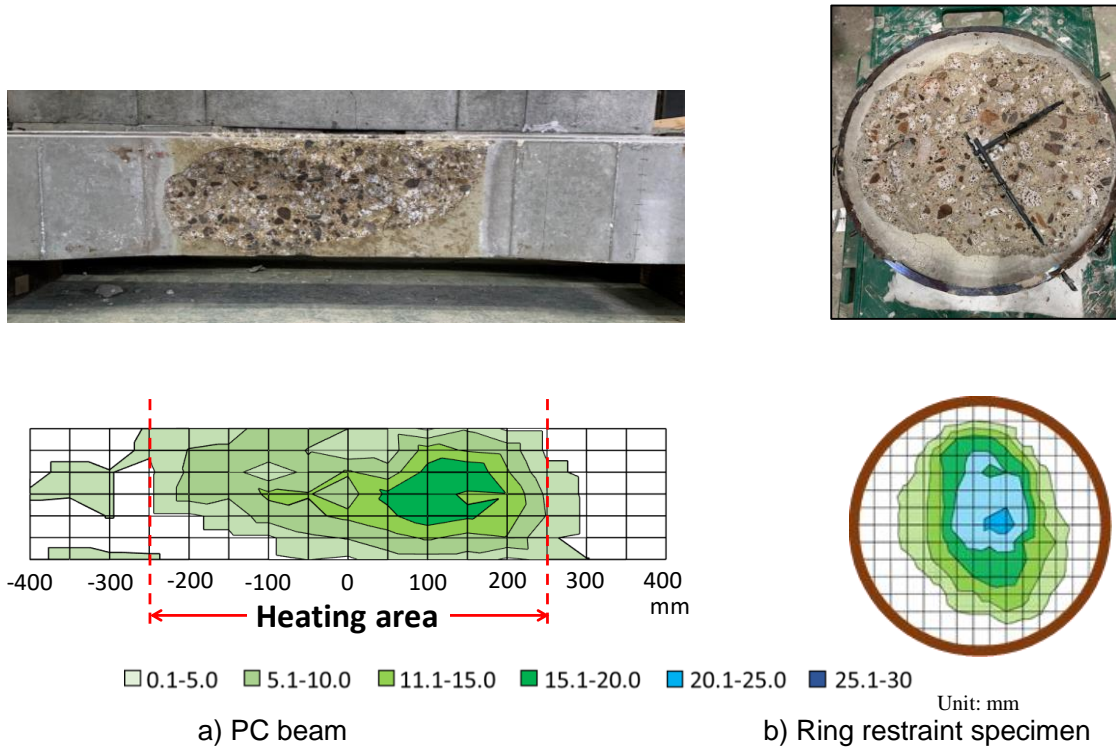


Fig. 5 The condition of the heating surface after heating, and the spalling depth contours

3.2 Evaluation of the fire spalling damage

Table 4 shows the evaluation of the fire spalling damage of the PC beam and ring restraint specimen following the JCI standard.

The maximum spalling depth was 19.9 mm and 26.0 mm for the PC beam and the ring specimen, respectively. All spalling grades were rated as D. The spalling area ratios were 58% and 78% for PC beams and ring specimens, respectively. All indexes were evaluated as E. The spalling volume ratios were 3.4% and 8.5% for the PC beam and ring specimen, respectively. The rating was C.

Although the evaluation of the index was the same for the PC beam and ring specimen, comparing the values, it can be seen that the ring specimen spalling damage is larger than that of the PC beam.

It is considered that the ring specimen was more damaged because the ring was multi-axial restraint while the PC beam was uni-axial restraint.

This trend is similar to that of a recent paper that shows results in the heating test at the ages of 3 months (Ikeya et al. 2019).

Compared to each index, the maximum spalling depth is rated D, because it is assumed that the cover to the tensile rebar is 30 mm. On the other hand, in the case of the PC beams, it is also necessary to evaluate by comparing the cover depth of the PC steel bar. The spalling area ratio was evaluated as the most damaged area. Because the area ratio is calculated based on the heated area, it is considered that the evaluation tends to be relatively high. On the other hand, the spalling volume ratio depends on the height of the

PC beam and ring specimen. This is because it is affected by the height of the specimen. The height of the ring specimen and PC beam were 100 mm and 160 mm, respectively. Therefore, it is considered that the spalling volume ratio was small. As mentioned above, although each spalling evaluation index was considered, it is necessary to evaluate it, including the cover to the rebar and the height of the specimen.

Table. 4 Evaluation of fire spalling damage

	The heating surface condition			Grade		
	Maximum spalling depth (mm)	Spalling area ratio (%)	Spalling volume ratio (%)	Index 1	Index 2	Index 3
PC	19.9	58.0	3.4	D	E	C
Ring	26.0	77.7	8.5	D	E	C

3.3 Internal temperature

Fig. 6 shows the temporal changes in the internal temperature of each specimen. In the PC beam (a), there is a rapid temperature increase point. The first rapid increase point was at a depth of 5 mm at 5.1 min. Similarly, at a depth of 5 mm, the temperatures increased rapidly at a depth of 10 mm. That is slower than at 5 mm and 10 mm, but the temperature increased even at a depth of 20 mm. The ring restraint specimen (b) exhibited a rapid increase in temperature at depths of 5 mm at 4.9 min after heating began. Then, the temperature began increasing rapidly at 10 mm and 25 mm, respectively. The rapidly increasing temperature of both specimens can be caused by fire spalling. It is considered that the thermocouple inside the concrete was exposed to the environment inside the gas furnace owing to the spalling of the concrete, which caused the temperature to rise rapidly. Altogether, it is considered that the time when the rapid temperature increasing occurred at each location is the time when the spalling occurred.

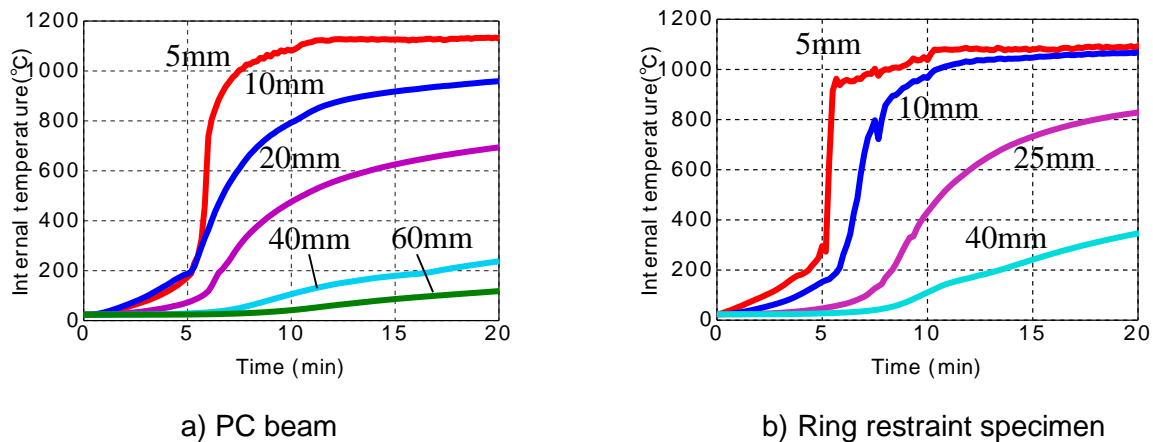


Fig. 6 Temporal changes in the internal temperature

3.4 Restraint stress

Fig. 7 shows temporal changes in restraint stress in the ring restraint specimen. The maximum restraint stress at a distance of 5 mm was 5 MPa at 10 min after heating began. Approximately 5 min from the start of heating, restraint stress temporarily decreased at depths of 5 mm and 10 mm. This is caused by the occurrence of fire spalling.

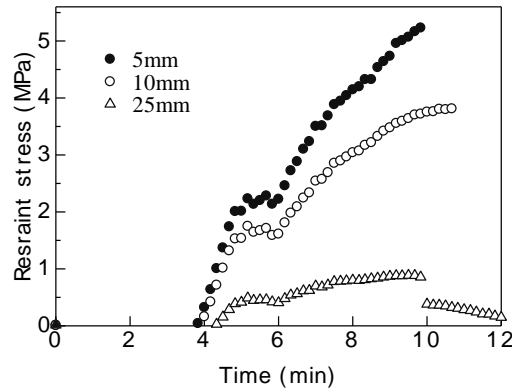


Fig. 7 Temporal changes in restraint stress in ring restraint specimen

3.5 Vapor pressure

Fig. 8 shows the temporal changes in the vapor pressure in the ring restraint specimen. The maximum vapor pressure at a depth of 5 mm was approximately 4.5 MPa. The vapor pressures rose sharply and then reduced at each measurement point. The rise in vapor pressure was sequential from the heating surface. The time when the vapor pressure decreased sharply matched that of when the internal temperature rose rapidly. This indicated that the vapor pressure increased due to the heating, and then the vapor was released to the outside by the spalling, and the vapor pressure dropped sharply.

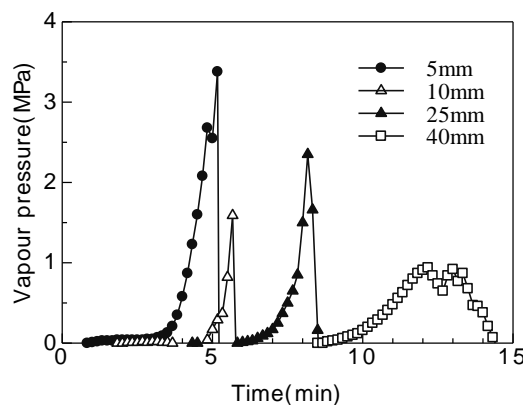


Fig. 8 Temporal changes in vapor pressure in the ring restraint specimen

3.6 Relation between restraint stress, vapor pressure, and internal temperature

Fig. 9 shows the relationship between the restraint stress, vapor pressure, and internal temperature at distances of 10 mm and 25 mm, and the saturated vapor pressure (SVP) curve. Ichikawa et al. have reported the relationship between vapor pressure and variations in temperature (the left of the SVP graph denotes the saturated zone and the right, the dry zone) (Ichikawa et al., 2004). The vapor pressure at 10 mm changed in the dry zone, and the maximum value was 1.6 MPa. At 25 mm, the value of the vapor pressure moved from the saturation zone at the beginning of heating. Jansson has reported that pore water moves from the heating surface to the inside of the concrete by heating (Jansson, 2013). In this case as well, it is considered that 10 mm near the heating surface was dry, while 25 mm was more humid due to the rise of water from the bottom. Next, the restraint stress has an inflection point. The value of the point at 10 mm was 1.8 MPa (160°C). The depth of 25 mm was 0.7 MPa (90°C). This is caused by the degradation of the elastic modulus and cracks associated with heating.

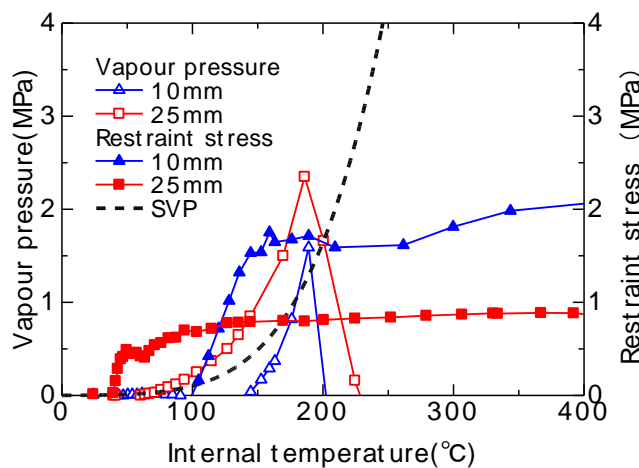


Fig. 9 The relation between the restraint stress, vapor pressure, and internal temperature in the ring restraint specimen (at 10 mm and 25 mm)

Fig. 10 shows an image of the fire spalling process occurring in the ring restraint specimen. First, the steel ring restrained the thermal expansion of the heated concrete. This causes compressive stress in the horizontal direction (x-direction) with the heating surface (1st phase). At the same time, tensile strain occurs in the perpendicular direction (z direction) by the apparent Poisson effect, and micro cracks occur in the concrete (2nd phase). Subsequently, vapor enters the fracture surface caused by the development of microcracks (3rd phase). It is considered that the fire spalling occurred because the vapor pressure increased in the fracture surface as the heating progressed. Fire spalling is assumed to proceed by repeating the process of the combined action of restraint stress and vapor pressure.

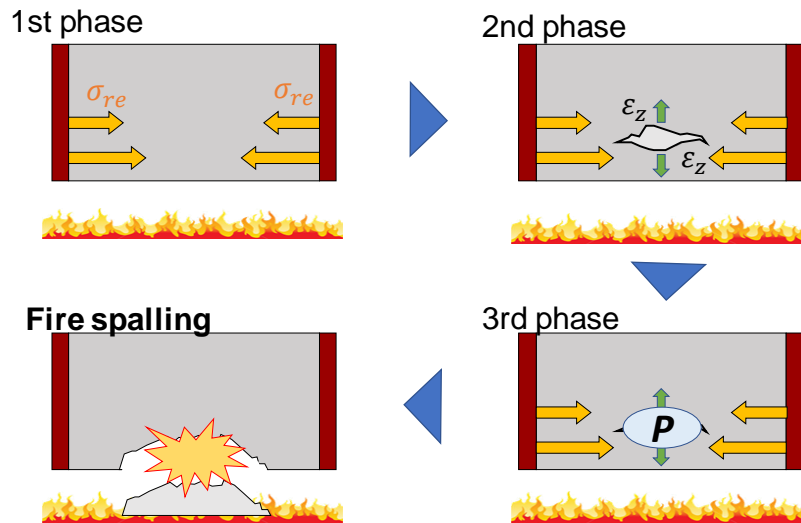


Fig.10 Illustration of the fire spalling process occurring in the ring restraint concrete specimen

3.7 Comparison of temporal changes in the fire spalling depth of the PC beam and ring restraint specimen.

Fig. 11 shows the temporal changes in explosive spalling depths of the PC beam and ring restraint specimen. The spalling beginning time and temporal changes in explosive spalling depths were similar for both fire tests. The maximum explosive spalling

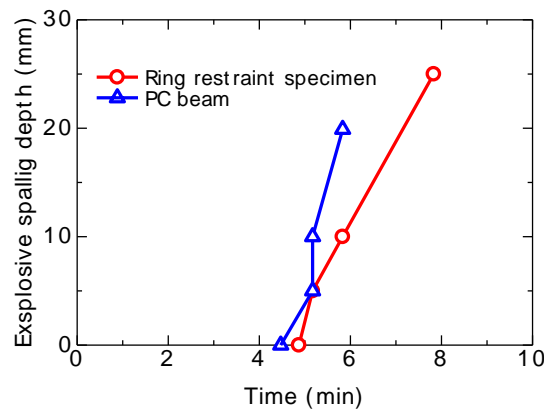


Fig. 11 Temporal changes in the explosive spalling depths of the PC beam and ring restraint specimen

*The 2020 World Congress on
The 2020 Structures Congress (Structures20)
25-28, August, 2020, GECE, Seoul, Korea*

depth for the PC beam was approximately 20 mm, whereas that of the ring restraint specimen was 26 mm. This was caused by the difference in the restraint type.

4. CONCLUSION

The results of this study can be summarized as follows:

- 1) In the PC beam and ring restraint specimen heating tests, the time when spalling began and the temporal changes in fire spalling were approximately similar. On the contrary, the maximum fire spalling depths of the ring restraint specimen were greater than those of the PC beam. This is because the PC beam was restricted in the uniaxial direction by the PC steel bar, whereas the ring restraint specimen was restricted in multi-axial directions by the steel ring.
- 2) We evaluated the fire spalling damage of the PC beam and ring restraint specimen following the JCI standard. As determined, the maximum spalling depth was 19.9 mm and 26.0 mm for the PC beam and the ring specimen, respectively. All spalling grades were rated as D. The spalling area ratios were 58% and 78% for PC beams and ring specimens, respectively. All indexes were evaluated as E. The spalling volume ratios were 3.4% and 8.5% for the PC beam and ring specimen, respectively. The rating was C. Although the evaluation of the index was the same for the PC beam and ring specimens, comparing the values, it can be seen that the spalling damage of the ring specimen is larger than that of the PC beam.
- 3) It was found that the ring restraint test is effective in allowing the quantitative examination of the fire spalling mechanism of concrete by temperature, restraint stress and vapour pressure.

REFERENCES

- Colin, G. B. and Ehab, E. (2009), "Fire tests on bonded post-tensioned concrete slabs", *Eng. Struct.*, **31**, 686-696.
- Gales, J., Bisby, L.A. and Gillie, M. (2011), "Unbonded post tensioned concrete in fire: A review of data from furnace tests and real fires", *Fire Saf. J.* **46**, 151-163.
- Na-Hyun, Y., Seung-Jai, C., Sang-Won, L. and Jang-Ho J. K. (2015), "Failure behavior of unbonded bi-directional prestressed concrete panels under RABT fire loading", *Fire Saf. J.*, **71**, 123-133.
- Fujimoto, K., Ozawa, M., Yamamoto, S. and Izutsu, K. (2018), "Explosive spalling behavior and load capacity of prestressed concrete members exposed to fire", The International Federation for Structural Concrete 5th International fib Congress 2018, 8-11 Oct. 2018, Melbourne, Australia.
- Ozawa, M., Tanibe, T., Kanematsu, M. and Morita T. (2017a), "Screening-test analysis of fire spalling behavior with various concrete samples", Proceeding of 5th International Workshop on Concrete Spalling due to Fire Exposure, 315-326.
- Japan concrete Institute (2018), "Test Method for Spalling of Concrete under High Temperature Exposure", JCI-S-014-2018
- Ozawa, M., Tanibe, T., Kamata, R., Uchida, Y., Rokugo, K. and Parajuli S. S. (2017b), "Behavior of ring-restrained high-performance concrete under extreme heating and development of screening test", *Constr. Build. Mater.*, **162**, 215-228.

The 2020 World Congress on
The 2020 Structures Congress (Structures20)
25-28, August, 2020, GECE, Seoul, Korea

- Akasaka, H., Ozawa, M., Parajuli, S.S., Sugino, Y., Akutsu, Y., Murakami, M., (2018), "Preventive effect on fire spalling of high-strength concrete with Jute fibre in ring-restraint specimen", Proceedings of the 14th International Conference on Concrete Engineering and Technology (CONCET 2018), August 7-10
- Ichikawa, Y. and England G. L. (2004), "Prediction of moisture migration and pore pressure build-up in concrete at high temperature", *Nucl. Eng. Des.*, **228**(1-3), 245-259.
- Jansson, R, (2013), "Fire Spalling of Concrete Theoretical and Experimental Studies", Doctoral Thesis in Concrete Structures, Stockholm, Sweden, pp. 18